Electron transport in the presence of a Coulomb field

Joachim Burgdörfer and John Gibbons
Department of Physics, University of Tennessee, Knoxville, Tennessee 37996-1200
and Oak Ridge National Laboratory, Oak Ridge, Tennessee 37831-6377
(Received 28 February 1990)

We analyze the modifications of the transport behavior of electrons in dense media due to the presence of a strong Coulomb field generated by an ion moving initially in close phase-space correlation with the electrons. These modifications play a profound role in convoy electron emission in ion-solid collisions. The transport behavior is studied within the framework of a classical phase-space master equation. The nonseparable master equation is solved numerically using test-particle discretization and Monte Carlo sampling. In the limit of vanishing Coulomb forces the master equation becomes separable and can be reduced to standard one-dimensional kinetic equations for free-electron transport that can be solved exactly. The comparison to free-electron transport is used to gauge both the reliability of test-particle discretization and the significance of Coulomb distortion of the distribution functions. Applications to convoy-electron emission are discussed.

I. INTRODUCTION

Recent experimental investigations of near-threshold excitation in fast ions transversing thin solid targets have revealed significant modifications of the excitation function compared to that observed in ion-atom scattering under single-collision conditions. Near-threshold excitation encompasses high Rydberg states just below threshold and convoy electrons, i.e., electrons in the low-energy continuum of the projectile just above the threshold. Convoy electrons give rise to the well known "cusp" shaped peak in the forward emission spectrum of electrons whose velocity vector $\mathbf{v}_e$ matches the projectile velocity $\mathbf{v}_P$, i.e., $\mathbf{v}_e \simeq \mathbf{v}_P$. Features that are clearly at variance with observations in gas-phase collisions under otherwise identical conditions of projectile charge state q and projectile velocity v_P include the abundant population of high-l Rydberg states,[1-6] the high-order multipole content of the convoy-electron velocity distributions,[7] and enhanced yields of convoy electrons that point to anomalous transport properties such as an enhanced transport length.[8-11].

It has become clear that a description of foil-excited states requires a detailed study of the dynamical evolution of the electronic states around swift ions inside the solid. More specifically, the observed final-state distribution is the result of a complex dynamical evolution of the electronic charge cloud associated with the swift ion which is governed by the interplay between multiple scattering in the medium and the electron-projectile Coulomb interaction. It goes without saying that the transient wave packet formed inside the solid has little in common with stationary atomic (or ionic) states. Nonetheless, the buildup of a closely phase-space-correlated, isotachic electron flow in the proximity of the projectile is a precursor event for the formation of post-foil Rydberg and convoy-electron states.

A theoretical description is complicated by the intrinsic complexity of the underlying interaction processes. Viewing the evolution in terms of transient projectile-centered states, one is faced with the problem of strong perturbations, both time dependent and time independent, which preclude any perturbations treatment. Time-dependent perturbations result from multiple scattering of the electron at target atoms while time-independent perturbations are due to the dynamical screening of the Coulomb field in the medium (the "wake" field[12,13]).

In the following we discuss a classical transport theory employing stochastic dynamics. At present, a quantum-mechanical transport theory appears to be a formidable, even though highly desirable, task in view of the large number of coupled states including those in the continuum. It is not at all obvious within which basis set of manageable size the evolution of the transient wave packet can be represented with sufficient accuracy. Corrections due to quantum effects are therefore an open question and presently under investigation. We focus here on the influence of the nearby Coulomb field on the transport of electrons. For technical and conceptual reasons we treat the electron-projectile interactions as purely Coulombic, thereby neglecting the dynamical screening field. Investigations performed in parallel employing the dynamical screening potential[14] show that the dynamical screening field alters the transport properties only weakly. This is due to the fact that the primary excitation process of convoy electrons, which provides the initial conditions for the transport problem, takes place at small distances where dynamical screening is not yet effective. The dynamical screening field plays, however, a crucial role in other aspects of ion-solid interactions, e.g., molecular dissociation[15] and the electron emission induced by antiproton transmission.[16] The conceptual advantage of using a pure Coulomb field lies in the fact that the modification of transport coefficients can be expressed in terms of universal scaled variables based on classical

similarity transformations. On a more technical level, the propagation in a Coulomb orbit in between subsequent collisions can be performed in terms of a discrete mapping rather than by numerically integrating the equations of motion as required for the wake potential.

Transport of free electrons (or other pointlike charged particles) through dense media is one of the few simple problems of transport theory. The transport behavior is determined by multiple scattering leading to both angular straggling and energy straggling of an initially well-collimated monoenergetic beam. The framework for the theoretical description of elastic and inelastic scattering, mostly treated separately, has been established some time ago.[17–24] Within our present description, free-electron transport can be recovered as the $q \to 0$ limit, i.e., in the limit of vanishing Coulomb force (q is the charge of the projectile). The free-electron limit will be used as a gauge for the modification of the transport behavior in the presence of a Coulomb force. Since the underlying transport equation, a phase-space master equation, can be solved exactly, though numerically, for free electrons, the numerical accuracy of the test-particle discretization and Monte Carlo sampling method used in solving the full transport problem can be tested. Furthermore, we will be in the position to test the separability assumption of angular and energy straggling underlying the standard theory of free-electron transport.

In Sec. II we briefly introduce the theoretical framework, the phase-space master equation, and classical stochastic dynamics. The transport kernels or differential inverse mean free paths (DIMFP's) entering the theory as input will be discussed in Sec. III. Results for free-electron transport will be presented in Sec. IV, followed by results for the electron transport in the presence of a Coulomb field in Sec. V, where implications for convoy-electron emission will also be discussed. Concluding remarks will be given in Sec. VI. Atomic units are used unless otherwise stated.

II. PHASE-SPACE MASTER EQUATION AND CLASSICAL STOCHASTIC DYNAMICS

A. Phase-space master equation

Within the framework of (nonrelativistic) classical dynamics ($v_P \ll c$) the electron transport problem in the presence of the field of the projectile ion moving with speed v_P is described by a phase-space master equation for the distribution function ρ,

$$\frac{\partial}{\partial t}\rho(\mathbf{r},\mathbf{v},t)=(\hat{L}+\hat{R})\rho(\mathbf{r},\mathbf{v},t)\ , \tag{1}$$

where

$$\hat{L}=-\mathbf{v}\cdot\nabla_r+\nabla V_P\cdot\nabla_v \tag{2}$$

is the classical Liouville operator describing the phase-space flow ("drift") due to the electron-projectile interaction V_P, and $\hat{R}$ is the collision operator. In (1) we have adopted the projectile frame as a Galilean frame of reference. Accordingly, the dynamical phase-space variables $(\mathbf{r},\mathbf{v})$ are defined relative to the projectile ion. The effective electron-projectile interaction V_P, which, in general, includes the dynamical screening potential,[14] will in the following be replaced by a bare Coulomb potential

$$V_P(\mathbf{r})=-\frac{q}{r} \tag{3}$$

for an ion of charge state q. The collision operator (relaxation operator) is given by

$$\hat{R}\rho=\int d^3P[\,W(\mathbf{v}_e-\mathbf{P},\mathbf{P})\rho(\mathbf{r},\mathbf{v}-\mathbf{P},t) - W(\mathbf{v}_e,\mathbf{P})\rho(\mathbf{r},\mathbf{v},t)\,] \tag{4}$$

where the transition rates $W(\mathbf{v}_e,\mathbf{P})$ depend on both the local momentum $\mathbf{v}_e$ of the electron at the time of the collision and the momentum transfer $\mathbf{P}$ during the collision. The transition rates are proportional to the differential inverse mean free path or differential cross sections. They describe both elastic and inelastic scattering with the target atoms or the delocalized electron gas of the medium. They play the role of a kernel of the linear integro-differential equation in six space and one time (6+1) dimensions. For reasons of clarity we express the velocity dependence of the DIMFP's in terms of the lab velocity $\mathbf{v}_e$ rather than in terms of the velocity in the projectile frame $\mathbf{v}=\mathbf{v}_e-\mathbf{v}_P$. The assumption of a homogeneous (i.e., $\mathbf{r}$ independent) kernel is justified for homogeneous media and, to a lesser extent, for amorphous targets or propagation along "random" directions in a solid. A detailed description of the W chosen in our calculation is given in Sec. III. Equation (1) is nonseparable due to the presence of the Coulomb interaction and due to the coupling of different degrees of freedom by the collision kernels. Separable approximations for the DIMFP's will be considered below.

The linearity of (1) in ρ is the result of a one-electron approximation: The "active" electron whose phase-space correlation with the ion is analyzed is well separated in phase space from the electrons in the medium since in our case $v_P \gg v_F$ (v_F is the Fermi velocity). The full Boltzmann-type collision integral can therefore be linearized yielding (4). It should be noted that (2) is still nonlinear in canonical phase-space variables $(\mathbf{r},\mathbf{v})$. The nonlinear and chaotic dynamics in the underlying single-particle motion is therefore present. Both $\hat{L}$ and $\hat{R}$ possess axial symmetry about the beam velocity ($\hat{v}_P$). If the initial conditions possess axial symmetry as well, Eq. (1) can be reduced to a (4+1)-dimensional integro-differential equation. Since even in reduced form this equation is not easily accessible to a direct numerical solution with present computing capabilities, we will use therefore an alternative approach employing classical stochastic dynamics and test-particle discretization as discussed below. In the latter form the dimensionality plays a less crucial role such that the full (6+1)-dimensional transport problem can be solved for initial conditions of arbitrary symmetry. We note that the time coordinate in (1) can be replaced by the path length of the projectile ion, which in a straight-line approximation is given by

$$Z=v_P t\ , \tag{5}$$

i.e., angular straggling and energy loss of the heavy particle is neglected, which is well justified in view of the small electron to nucleus mass ratio ($\lesssim 10^{-3}$). We will in the following use path length and time interchangeably. It should be noted that the path length of the accompanying electron does not coincide with the one of the ion Z. In the present case this is not primarily due to the well-known path-length enhancement due to electronic angular straggling in free-electron transport,[25] but due to Coulomb potential induced trajectory effects. The latter turn out to be far more important, in particular for highly charged ions, while the former will be neglected.

B. Initial conditions

The determination of the initial condition, i.e., $\rho_0=\rho(\mathbf{r},\mathbf{v},Z=0)$, relies on specific models for atomic collisions which are considered to be responsible for the formation of projectile-centered near-threshold states. The primary excitation event requires a large momentum transfer in a close collision and therefore closely resembles binary ion-atom collisions. Two processes are important for formation of final states near threshold: electron capture predominantly from inner shells of the target or direct excitation of a low-lying projectile state of an electron either carried into the collision or formed in an earlier stage of the transmission. The extension of these processes to continuum states are known as electron capture to continuum (ECC) and electron loss to continuum (ELC), respectively.[26] Realistic distribution functions can be derived from experimentally determined cross sections for capture and excitation. Alternatively, phase-space distributions can be taken from classical trajectory Monte Carlo (CTMC) calculations[27] for binary ion-atom collisions. In the present investigation of near-threshold excitation in the Coulomb field, we use a constrained microcanonical distribution function of well-defined angular momentum

$$\rho_0(E,L,\mathbf{r},\mathbf{v})=N(E,L)\delta(E-v^2/2+q/r)\delta(L-|\mathbf{r}\times\mathbf{v}|)\ , \tag{6}$$

where $N(E,L)$ is a suitably chosen weighting function such that ρ_0 is normalized to excitation or capture probabilities. For example, the n^{-3} rule for excitation cross sections is incorporated into (6) by requiring that after integrating over $\mathbf{r}$ and $\mathbf{v}$, $\rho_0(E,L)$ is a constant near threshold as a function of E. Similarly, the dominance of low angular momenta in the final-state population formed in fast ion-atom collisions is modeled by a distribution function $\rho_0(E,L)$, which peaked at small values of L. The distribution function (6) corresponds to an isotropic ensemble. Gas-phase studies of ECC and ELC show that cusp electron emission displays anisotropies.[26,28] Extensions to anisotropic ensembles using specific distribution functions for Euler angles (see Sec. II C) are straightforward.

For cusp electrons in the Coulomb continuum ($E\gtrsim 0$), which will be studied in the following, an additional radial constraint of the coordinate space is needed since the motion is unbounded. We construct a normalizable distribution function by introducing a cutoff. For ion-solid collisions such a radial cutoff $r<r_c$ is naturally provided by the requirement of a large momentum transfer and, in turn, a close collision in order to transfer an inner-shell electron into the continuum. For loosely bound electrons the dynamical screening length λ_D, within which the electron-projectile interaction is only effective, provides an additional less restrictive cutoff. We will parametrize the cutoff for cusp electrons with $E=0$ and fixed L in terms of a multiple α of the minimum distance of closest approach (the pericenter distance),

$$r_c=\alpha r_{\min}=\alpha\frac{L^2}{2q}\ . \tag{7}$$

In the following numerical studies we will choose $\alpha=10$. The resulting distribution function

$$\rho_0(E=0,L,\mathbf{r},\mathbf{v})=N(L)\delta\left[\frac{q}{r}-v^2/2\right]\times\delta(L-|\mathbf{r}\times\mathbf{v}|)\Theta\left[\alpha\frac{L^2}{2q}-r\right]\ ,$$

with $N(L)=N(E=0,L)$ leads, for fixed cutoff parameter α, to a universal distribution function in momentum space

$$\begin{aligned}\rho_0(E=0,L,\mathbf{v})&=\int d^3r\,\rho_0(E=0,L,\mathbf{r},\mathbf{v})\\&=N(L)(v/p_0)^{-4}\frac{1}{(p_0^2-v^2)^{1/2}}\\&\quad\times\Theta(p_0-v)\Theta\left[v-\frac{p_0}{\sqrt{\alpha}}\right]\ ,\end{aligned} \tag{8}$$

which depends on q and L only through the characteristic momentum

$$p_0=\frac{2q}{L} \tag{9}$$

of the classical cusp electron, i.e., of the parabolic orbit in the Coulomb field (Fig. 1). p_0 plays the role of a classical analog to the Compton width of the $E=0$ quantum state. In the initial distribution in the close collision regime $t=0$, $v=0$ electrons are absent since $v\geq p_0/\sqrt{\alpha}$, a consequence of the radial cutoff. The peak at $v=0$ develops, however, as $t\to\infty$ (or equivalently, $Z\to\infty$) under the influence of $\hat{L}$ without any collisional interaction ($\hat{R}=0$) since Eq. (8) represents the population of $E=0$ threshold states. In Fig. 1 the radial momentum distribution at $t=0$ (Eq. 8) is shown for $\alpha=10$ as a function of the reduced variable v/p_0 together with its Monte Carlo simulation discussed below. The distribution is peaked at the low cutoff $p_0/\sqrt{\alpha}$ and will eventually shift to $v=0$ as $t\to\infty$. We emphasize that all velocity distributions as a function of path length discussed in the following refer to the *asymptotic* velocity distribution (i.e., to the $t\to\infty$ limit in the collision-free regime outside the foil) after propagating a finite path length Z or the corresponding time of evolution $t(Z)$ under the influence of multiple scattering ($\hat{R}\neq 0$) inside the medium.

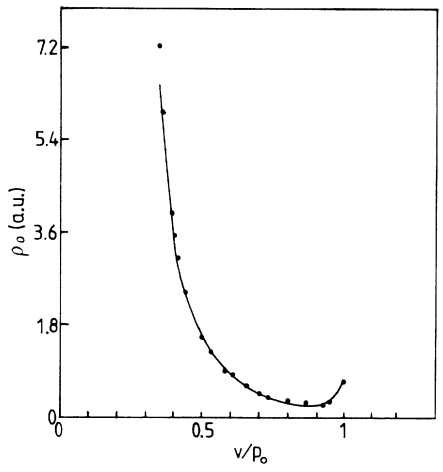

FIG. 1. Initial momentum distribution $\rho_0(E=0,L,v)$ of a classical cusp electron in units of reduced momentum variable $p_0=2q/L$. Scaling parameter for radial cutoff $\alpha=10$. —— Eq. (8); ● Monte Carlo simulation of initial conditions.

C. Test-particle discretization and classical stochastic dynamics

Our method to solve the transport equation by a computer simulation involves two major ingredients: the representation of the phase-space distribution function ρ by an ensemble of representative test particles ("test-particle discretization") and the construction and solution of a stochastic differential equation. This equation of motion for the test particle should mirror the dynamics embodied in the transport equation (1) as closely as possible.

The construction of the initial conditions for orbits of test particles employs the Kepler equations in terms of eccentric anomaly[29] u. For $E=0$ orbits they read

$$\theta=\frac{u}{2}\left[1+\frac{u^2}{3}\right], \tag{10a}$$

$$r(u)=\frac{L^2}{2q}(1+u^2), \tag{10b}$$

$$x(u)=\frac{L^2}{2q}(1-u^2), \tag{10c}$$

$$y(u)=\frac{L^2}{q}u, \tag{10d}$$

$$\theta=\omega_\infty t+\theta_0, \tag{10e}$$

$$\omega_\infty=\frac{q^2}{L^3}, \tag{10f}$$

$$v_x=-p_0\frac{u}{1+u^2}, \tag{10g}$$

$$v_y=\frac{p_0}{1+u^2}, \tag{10h}$$

where the x-y plane is chosen to coincide with the orbital plane. Similar equations for negative-energy states (ellipses) and positive-energy states (hyperbolas) are given in the Appendix. The equal *a priori* assumption of the microcanonical ensemble implies a uniform distribution of the phase angle θ, the mean anomaly, which is realized by drawing uniformly distributed random numbers. The constraint $r<r_c$ is easily incorporated by rejecting all eccentric anomalies as determined from (10a) which would lead to $r(u)>r_c$ in (10b). Finally, the assumption of isotropy is incorporated by drawing random numbers for the three Euler angles for the rotation matrix, which transforms the coordinates of the orbital frame [Eq. (10)] into the projectile frame where $\hat{\mathbf{z}}\|\mathbf{v}_P$. The Euler angles[30] α and γ are uniformly distributed random numbers while β is uniform in $\cos\beta$. The resulting Monte Carlo (MC) simulation for the initial radial momentum distribution is shown in Fig. 1 together with the analytic theory [Eq. (8)].

The equation of motion governing the evolution of the initial conditions of test particles is a stochastic differential equation of the Langevin type,[31]

$$\frac{d}{dt}\mathbf{v}=-q\frac{\mathbf{r}}{r^3}+\mathbf{F}(t), \tag{11}$$

where $\mathbf{F}(t)$ is a stochastic force describing the collisional momentum transfer. Sampling the phase-space distribution of the test particles evolved according to (11) yields an approximate distribution function at a later time $\rho(t)$. The resulting distribution function is, within the limits of the Monte Carlo statistics, the exact solution of the transport problem.

Since the drift term in (11) agrees with the classical Liouville operator [Eq. (2)], the only nontrivial part in establishing the Langevin equation associated with the original transport problem lies in the calculation of stochastic force $\mathbf{F}$. Such a construction is clearly not unique. Our strategy is to optimize the agreement with the collision operator for a finite number of low-order jump moments,

$$\frac{d}{dt}\langle P_m^n\rangle=\int d^3P\,P_m^n\,W(\mathbf{v},\mathbf{P})\quad(m=z\text{ or }x). \tag{12}$$

Jump moments in x and y are equal because of axial symmetry. We note that in our application jump moments are not necessarily small compared to the characteristic momentum p_0 [Eq. (9)]. The reduction of the master equation to a Fokker-Planck equation[31] is therefore not applicable. For the same reason the term "diffusion" used in the following is not to be taken literally.

We describe the stochastic force in terms of a sequence of impulsive momentum transfers ("kicks"),

$$\mathbf{F}(t)=\sum_{\alpha=e\text{ or }i}\sum_j\Delta\mathbf{P}_j^\alpha\delta(t-t_j^\alpha), \tag{13}$$

where $\Delta\mathbf{P}_j^\alpha$ is the stochastic momentum transfer per collision at the time t_j^α. The determination of $\mathbf{F}(t)$ is thereby reduced to that of a stochastic sequence of pairs $(\Delta P_j^\alpha,t_j^\alpha)$. In (13) we have decomposed the stochastic sequence into independent subsequences. One sequence ($\alpha=e$) refers to elastic electron-target core scattering while the other ($\alpha=i$) refers to inelastic electron-electron

scattering. The terms (in)elastic refer here to (non)conservation of the kinetic energy of a scattered fast *free* electron. We note for later reference that in the presence of a Coulomb field the latter interpretation of this decomposition will lose its meaning.

The explicit determination of the stochastic sequences $(\Delta P_j^\alpha, t_j^\alpha)$ depends on the choice of the collision kernel in the master equation and will be discussed in Sec. III. The fundamental approximation underlying (13) is the assumption of an impulsive, instantaneous momentum transfer. It is based on the observation that collisional interaction with target atoms in the solid are short ranged and determined by the static screening length in the medium (typically of the order of 1 a.u.). This is to be distinguished from the dynamical screening length λ_D for the fast projectile, which is much larger. Dynamical screening is neglected in the following. The corresponding collision time $t_c \approx 1/v_P$ is small compared to the orbital period. For bound states the latter can be estimated to be of the order of $T_n = 2\pi n^3/q^2$. For cusp electrons a characteristic classical frequency is ω_∞ [see Eq. (10f)] and $T_\infty = 2\pi L^3/q^2$. The impulse approximation is therefore valid for a wide range of q, n, and L. Nonetheless, the introduction of unphysical high-frequency components via (13) may lead to an overestimate of strongly inelastic processes. Polarization effects of the target can be incorporated in the wake potential. Using Eq. (13), the Langevin equation can be integrated to give a discrete Coulomb mapping relating the canonical coordinates at the times of adjacent kicks. Denoting the values of the coordinates just prior to the jth kick by $(\mathbf{r}_j, \mathbf{v}_j)$ and those just prior to the $(j+1)$th kick by $(\mathbf{r}_{j+1}, \mathbf{v}_{j+1})$, we find the nonlinear mapping T,

$$\begin{pmatrix} \mathbf{r}_{j+1} \\ \mathbf{v}_{j+1} \end{pmatrix} = T \begin{pmatrix} \mathbf{r}_j \\ \mathbf{v}_j \end{pmatrix} , \tag{14}$$

where T can be decomposed as

$$T = T_0(\Delta t_j) T_c(\Delta \mathbf{P}_j^\alpha) , \tag{15}$$

with

$$T_c(\Delta \mathbf{P}_j^\alpha) \begin{pmatrix} \mathbf{r} \\ \mathbf{v} \end{pmatrix} = \begin{pmatrix} \mathbf{r} \\ \mathbf{v} + \Delta \mathbf{P}_j^\alpha \end{pmatrix} , \tag{16}$$

and $T_0(\Delta t_j)$ describing the evolution of canonical coordinates after the kick on unperturbed Coulomb orbits during a time interval Δt_j between adjacent kicks. Explicit calculation of $T_0(\Delta t_j)$ requires only the solution of the Kepler equations [Eqs. (10) and (A1)–(A18)] rather than a numerical integration. Assume, e.g., that $T(\Delta P_j^\alpha)$ generates an $E=0$ orbit with angular momentum L. The phase angle of the orbit will then change during the interval Δt_j by an amount $\Delta\theta_j = \omega_\infty \Delta t_j$. By solving the third-order Kepler equation [Eq. (10a)] the change in eccentric anomaly Δu_j and consequently the new canonical coordinates $(\mathbf{r}_{j+1}, \mathbf{v}_{j+1})$ can be determined [Eqs. (10b)–(10h)]. Obviously, for orbits with $E<0$ or $E>0$, the Kepler equations for bound states (ellipses) [Eqs. (A1)–(A10)] and for positive-energy states (hypobolas) [Eqs. (A11)–(A18)] must be used. This method allows the time-efficient propagation of relatively large ensembles (10^4–10^5 test particles) for several hundred collisions per particle.

D. Free-electron transport

The well-known transport equations for free electrons, i.e., in the absence of a perturbing Coulomb field, can be recovered from (1) in the limit $q \to 0$ as

$$\frac{\partial}{\partial t} \rho(\mathbf{v}, t) = \hat{R} \rho(\mathbf{v}, t) . \tag{17}$$

Note that in the absence of a field and for a homogeneous collision kernel the position coordinates is cyclic. The initial conditions of an initially well-collimated beam with $\mathbf{v}_e = \mathbf{v}_P$ (i.e., with a velocity distribution corresponding to an $E=0$ cusp electron) is given in the Galilean frame of the projectile by

$$\rho_0(\mathbf{v}) = N \delta(\mathbf{v}) . \tag{18}$$

For a comparative analysis of free-electron transport and transport in a Coulomb field it is important to realize that the limit $q \to 0$ requires both an alteration of the transport equation and of the initial conditions. A "mixed" treatment with (18) as initial conditions and the use of the master equation including the Coulomb field (1) is unsatisfactory since it induces unphysical transitions due to energy nonconservation unless an adiabatic switching procedure for the field is employed. We use therefore Eqs. (17) and (18) for free electrons and Eqs. (1) and (8) for electrons in the Coulomb field. The smooth transition between the two cases can be simulated by choosing small but finite values of q such that p_0 is small compared to the average collisional momentum transfer

$$p_0 \ll |\langle \Delta \mathbf{P} \rangle| . \tag{19}$$

The treatment of the free-electron transport within the framework of classical stochastic dynamics requires only minor changes. The drift term in the Langevin equation [Eq. (11)] vanishes for $q=0$ and the initial conditions of the ensemble of test particles is chosen as $\mathbf{v}=\mathbf{0}$ according to (18) with $\mathbf{r}$ arbitrary. Accordingly, $T(\Delta \mathbf{P}_j^\alpha)$ [Eq. (16)] remains unchanged while the map describing Coulomb evolution T_0 is replaced by the map describing free-particle evolution

$$T_f(\Delta t_j) \begin{pmatrix} \mathbf{r}_j \\ \mathbf{v}_j \end{pmatrix} = \begin{pmatrix} \mathbf{r}_j + \Delta t_j \mathbf{v}_j \\ \mathbf{v}_j \end{pmatrix} . \tag{20}$$

III. COLLISION KERNELS

Several approximations to kernels of the collision integral in (4) have been discussed for free-electron transport.[17–25,32,33] In most cases a separability approximation is invoked such that the free-particle master equation

$$\begin{aligned} \frac{\partial}{\partial t} \rho(v_e, \theta, t) &= \int dv' \int d\theta' (\sin\theta') \\ &\times [W(v_e - v', v', \theta') \rho(v_e - v', \theta - \theta', t) \\ &\quad - W(v_e, v', \theta') \rho(v_e, \theta, t)] \end{aligned} \tag{21}$$

reduces to two one-dimensional equations in the polar angle θ and v (or energy). Equation (21) follows from (17) upon eliminating the cyclic azimuthal angle. For free electrons we choose the conventional laboratory frame variables (v_e,θ). As before, the kernel is assumed to be homogeneous, i.e., **r** independent, corresponding to a homogeneous or "random" medium. The separable kernel reads[32]

$$W(v_e,v',\theta')=W_i(v_e,v')\delta(\cos\theta'-1)+W_e(v_e,\theta')\delta(v'), \tag{22}$$

expressing the fact that angular straggling is primarily due to elastic scattering and energy straggling due to inelastic scattering. A further approximation, valid only for small distances of propagation, assumes that the collision kernel is independent of the local speed of the scattered particles, i.e.,

$$\begin{aligned} W_i(v_e,v')&=W_i(v_P,v')\ , \\ W_e(v_e,\theta')&=W_e(v_P,\theta')\ , \end{aligned} \tag{23}$$

since $v_e(t=0)=v_P$. In this form the resulting one-dimensional master equations correspond to the Landau theory for energy straggling and the Goudsmit-Saunderson theory for angular straggling which can be solved exactly.[18,19] The solutions will be used to test the Monte Carlo simulations. Extensions using the continuous-slowing-down approximation to account for changes in the kernel due to changes in the velocity distribution are straightforward.[23] In stochastic dynamics calculation the approximation (23) is dispensable. The calculations therefore remain valid for larger distances of propagation, i.e., thicker foils. Furthermore, the approximation (22) is dispensable as well, which permits testing of the accuracy of the separability assumption.

In our calculation we choose collision kernels which are sufficiently simple to allow for a CPU time efficient drawing of nonuniform random number distributions and yet are physically acceptable approximations. For the elastic scattering ($\alpha=e$) we calculate W_e from scattering at an exponentially screened Coulomb potential $V(r)=-Z_T\exp(-r/a)/r$ with a Thomas-Fermi screening radius $a=0.886Z_T^{-1/3}$ and Z_T the charge of the target nucleus ($Z_T=6$ for carbon). In the first-order Born approximation we have

$$W_e(v_e,\theta)=\frac{\pi Z_T^2 n}{2v_e^3}\frac{1}{[\sin^2(\theta/2)+(1/2av_e)^2]^2}\ , \tag{24}$$

where n is the number density of target atoms.

Equation (24) has been shown to reproduce angular straggling of free electrons reasonably well.[32] A discussion of improved elastic kernels is given by Ganachard and Cailler[34] and Kwei.[24] Expressed in terms of the momentum transfer ΔP^e,

$$\Delta P^e=2v_e\sin(\theta/2)\ , \tag{25}$$

Eq. (24) reads

$$W_e(v_e,\Delta P^e)=\frac{8\pi Z_T^2 n}{v_e^2}\frac{\Delta P^e}{[(\Delta P^e)^2+(1/a)^2]^2}\ . \tag{26}$$

The distribution of target atoms (scattering centers) with medium is assumed to be random.

For the inelastic electron-electron scattering Ashley *et al.*[22] have provided a description of the kernel for carbon taking into account particle-hole and plasmon excitation. They express the kernel in terms of the dielectric function $\epsilon(\bar{q},\omega)$ as

$$W_i(v_e,v'(\omega))=\frac{2}{\pi v_e}\int d\bar{q}\ 1/\bar{q}\ \mathrm{Im}\left[\frac{-1}{\epsilon(\bar{q},\omega)}\right]\ , \tag{27}$$

with $\omega=(v')^2/2$ and use an approximation for $\epsilon(\bar{q},\omega)$ in terms of Drude-type functions,

$$\mathrm{Im}\left[\frac{-1}{\epsilon(\bar{q},\omega)}\right]=\sum_{i=1}^{4}\frac{A_i\gamma_i\omega_i}{[(\omega_{0i}+\bar{q}^2/2)^2-\omega^2]^2+(\gamma_i\omega)^2}\ . \tag{28}$$

The coefficients A_i, ω_{0i}, and γ_i are fitted to match the experimental optical energy-loss function $\mathrm{Im}[-\epsilon(\bar{q}=0,\omega)]^{-1}$. This approximation leads to reasonable agreement for the inelastic mean free path[22] and stopping power[32] of free electrons in the energy range of ≈ 1 keV, which we are primarily interested in. Bichsel has recently discussed various more sophisticated inelastic collision kernels including K-shell contributions.[33] The use of Eqs. (27) and (28) is particularly convenient for the numerical determination of the stochastic force. We note, however, that more elaborate input can be used if desired or necessary.

The calculation of the stochastic sequences $(\Delta\mathbf{P}_j^\alpha,\Delta t_j^\alpha)$ proceeds as follows. The collision kernels (26) and (27) determine the (in)elastic mean free path (MFP) for free electrons, $\lambda_{e,i}$

$$\frac{1}{\lambda_e}=\frac{1}{v_e}\int_0^\pi d\theta(\sin\theta)W_e(v_e,\theta)\ , \tag{29a}$$

$$\frac{1}{\lambda_i}=\frac{1}{v_e}\int_0^{(1/2)v_e^2-\epsilon_F}d\omega\ W_i(v_e,v'(\omega))\ . \tag{29b}$$

From (29), the average time interval between two adjacent collisions (reciprocal of the collision frequency) of the same type ($\alpha=e,i$) follows as

$$\langle\Delta t_j^\alpha\rangle=\lambda_\alpha/v_e\ . \tag{30}$$

In the following numerical study $\langle\Delta t_j^\alpha\rangle\simeq 4$ a.u. For a homogeneous (or random) medium the stochastic point process is Poissonian.[31] Consequently, the probability distributions in Δt_j^α are given by

$$\begin{aligned} P(\Delta t_j^\alpha)&=\exp(-\Delta t_j^\alpha/\langle\Delta t_j^\alpha\rangle) \\ &=\exp(-v_e\Delta t_j^\alpha/\lambda_\alpha) \end{aligned} \tag{31}$$

with the two sequences ($\alpha=e$ or i) assumed to be independent of each other.

The probability distributions for the elastic momentum transfers per collisions are given (up to an irrelevant normalization constant) by

$$P(\Delta\mathbf{P}^e)=W_e(v_e,\Delta P^e)\ . \tag{32}$$

Note that the magnitude ΔP_e defines the polar angle of the vector $\Delta \mathbf{P}_i$ through (25) while the azimuthal angle ϕ is cyclic. The latter is to be uniformly randomized in the interval $[0,2\pi]$ in view of axial symmetry.

We encounter a different situation for inelastic scattering processes: The kernel $W(v_e,v'(\omega))$ (27) determines only the longitudinal momentum transfer v', more precisely, the momentum transfer antiparallel to the beam velocity $\Delta P_{\parallel}^i$. The latter is directly related to the stopping power

$$\frac{dE}{dx}=\frac{1}{v_e}\int_0^{(1/2)v_e^2-\epsilon_F} d\omega\,\omega W_i(v_e,v'(\omega))=\langle\omega\rangle/\lambda_i \tag{33}$$

since

$$\langle\omega\rangle\simeq\langle\Delta P_{\parallel}^i\rangle v_e\ . \tag{34}$$

Recoil kinematics requires, however, that the inelastic scattering process is also associated with a transverse momentum transfer. This applies to both particle-hole excitations and collective excitations. For example, Raether[35] points out that plasmon emission by fast electrons occurs in predominantly transverse direction. This transverse momentum transfer associated with stopping and straggling is to be distinguished from the well-known transverse contribution to stopping in the relativistic case due to virtual photons.[20] The presence of a transverse component $\Delta P_{\perp}$, which is, in fact, larger than $\Delta P_{\parallel}$, destroys the separability of the kernel W [Eq. (22)]. Its quantitative importance will be investigated in Sec. IV. The full vectorial momentum transfer due to the dielectric response can be derived from the inverse dielectric function itself rather than from the integral (27), i.e.,

$$P(\Delta\mathbf{P}^i)=\frac{1}{\Delta P^i}\mathrm{Im}\left[\frac{-1}{\epsilon(\Delta P^i,\omega)}\right], \tag{35}$$

and the kinematic relation

$$\tfrac{1}{2}v_e^2=\tfrac{1}{2}(\mathbf{v}_e-\Delta\mathbf{P}_i)^2+\omega\ . \tag{36}$$

Accordingly, the longitudinal and transverse momentum components are given by

$$\Delta P_{\parallel}^i=-\left[\frac{(\Delta P^i)^2}{2v_e}+\frac{\omega}{v_e}\right], \tag{37}$$

$$\Delta P_{\perp}^i=[(\Delta P^i)^2-(\Delta P_{\parallel}^i)^2]^{1/2}\ . \tag{38}$$

Equation (35) amounts to a two-dimensional nonuniform distribution of random numbers. The function $\mathrm{Im}(-\epsilon(\bar{q},\omega))^{-1}$ entering (35) is depicted in Fig. 2. It should be remarked that a plasmon dispersion relation $\omega(\Delta P)$ in carbon is only poorly defined because of the width of the plasmon peak ($\sim$0.5 a.u.). As is the case for the elastic scattering, the cyclic azimuthal angle is uniformly distributed.

Figures 3 and 4 display the collision kernels [or (DIMFP's)] for inelastic and elastic scattering. Figure 3 shows the DIMFP associated with the longitudinal momentum transfer in the inelastic process. The agreement between the analytic expression for (27) derived by Ashley *et al.*[22] and the MC simulation is excellent. The collision kernel for angular scattering (Fig. 4) displays a new feature. In addition to the DIMFP for angular scattering by elastic scattering, we find a DIMFP for angular scattering by inelastic scattering. The complete differential angular scattering probability is then a convolution of the two distributions. The agreement between the analytic expression and the MC simulation for the elastic DIMFP is excellent. For the angular scattering due to inelastic scattering no analytic expression is available. The MC simulation shows that the latter is strongly peaked in forward direction. Angular straggling for free electrons is clearly dominated by the elastic channel thereby justifying the separability assumption (22) for many applications. However, the angular straggling contribution from the inelastic channel will play an important role in the presence of a Coulomb field.

The present method allows the construction of stochastic forces such that the distribution function of the en-

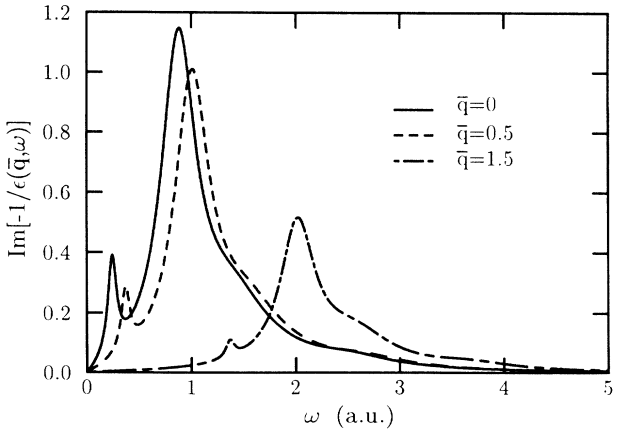

FIG. 2. Inverse dielectric function for carbon $\mathrm{Im}\{-1/[\epsilon(\bar{q},\omega)]\}$ according to Eq. (28) as a function of ω for different wave numbers $\bar{q}$.

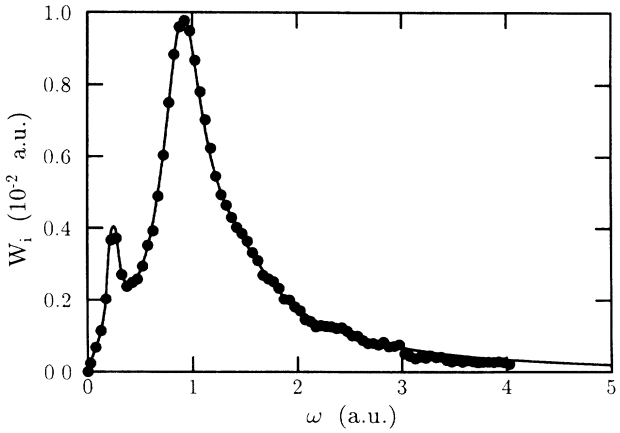

FIG. 3. Collision kernel W_i [——, Eq. (27)] for energy loss (or longitudinal momentum transfer); ● Monte Carlo simulation.

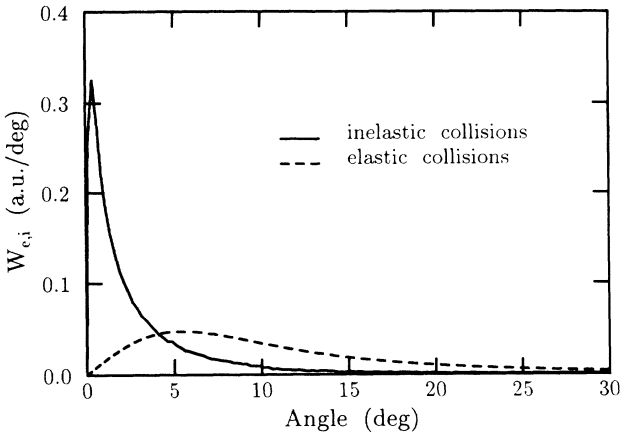

FIG. 4. Collision kernels for angular straggling due to elastic collisions, W_e [Eq. (24)], and due to inelastic collisions W_i [Eq. (32)].

semble of "kicks" reproduces the kernels very accurately. The agreement can be measured in terms of the moments of the kernel [Eq. (12)]. The zeroth-order moments which give the collision rates [or equivalently, the MFP's, Eq. (29)] are automatically reproduced by choosing $P(\Delta t_j^\alpha)$ distributions according to Eq. (31). The first-order moment for longitudinal momentum transfer gives the stopping power [Eq. (33)] while the second moments measure energy and angular straggling,

$$\frac{d(\Delta E)^2}{dx}=\frac{1}{v_e}\int_0^{(1/2)v_i^2-\epsilon_F} d\omega\,\omega^2 W_i(v_e,v'(\omega)) , \tag{39}$$

$$\frac{d\theta^2}{dx}=\frac{1}{v_e}\int_0^{\pi} d\theta(\sin\theta)\theta^2 W_e(v_e,\theta) . \tag{40}$$

In all cases, we find good agreement between the analytic theory and the MC simulation. Deviations due to statistical fluctuations were $\lesssim 5\%$.

IV. FREE-ELECTRON TRANSPORT

Free-electron transport is used to test the classical stochastic dynamics approach for a case where an exact (numerical) solution to the master equation exists. Monte Carlo methods have been used primarily[36] for solving one-dimensional master equations in the separable limit. The present method treats the full six-dimensional phase-space evolution. The price to pay is that the statistics per degree of freedom is significantly reduced. Upon tracing out all unobserved degrees of freedom the agreement with the exact solution for free-electron transport is excellent.

We have compared the evolved distribution with the numerical solutions of the Landau and the Goudsmit-Saunderson theory of energy straggling and angular straggling [Eqs. (21)–(23)]. The full six-dimensional phase-space distribution is projected onto the energy and angle axes. The following limitations in the validity of this comparison should be noted: The Landau and Goudsmit-Saunderson theories assume a velocity-independent kernel [Eq. (23)]. We confine therefore the comparison to small distances of propagation $d\lesssim 450$ a.u. ($\simeq 240$ Å), which is also the most interesting region for the study of Coulomb-field-induced modifications. For larger distances path-length modifications due to angular straggling become important. Furthermore, in the separable approximation [Eq. (22)] the angular straggling due to inelastic processes is neglected. We correct for this by convoluting two independent angular straggling distributions each calculated using the Goudsmit-Saunderson theory and the kernels for elastic [Eq. (26)] and inelastic scattering [Eq. (35)], respectively. Finally, the solutions [Eqs. (21)–(23)] yield energy and angular distributions at fixed distances of propagation while the MC simulations yield phase-space distributions for a fixed number of time steps of evolution. Since the latter implies a distribution rather than a sharp value for the path length, the equivalence is strictly fulfilled for ensemble expectation values while deviations in the tails of the distribution functions occur.

Figures 5(a)–5(c) show the energy distribution of an in-

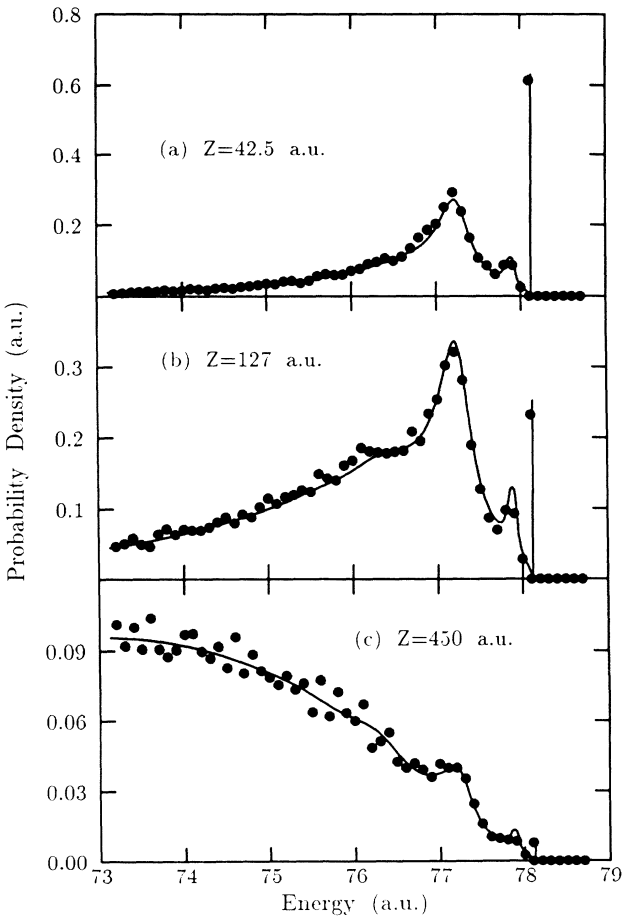

FIG. 5. Energy straggling distribution in laboratory frame for free electrons and path length (a) $Z=42.5$, (b) $Z=127$, and (c) $Z=450$ a.u.; ——, Landau theory; ●, Langevin equation (bin size $\Delta E=01$ a.u.). The zero-scattering peak represents a probability.

itially monoenergetic beam of electrons with $v_e = v_P = 12.5$ a.u. and the values for the path length $Z = 42.5$, 127, and 450 a.u. A bin size on the energy scale of $\Delta\varepsilon = 0.1$ a.u. is used. For the shortest distance of propagation the plasmon peaks due to σ and π electrons (at $E \simeq 77.2$ and 77.8 a.u.), as well as a shoulder due to the onset of double plasmon excitation ($E \simeq 76.1$ a.u.), are clearly visible. The majority of all test particles (=60%) remains in the zero-scattering bin corresponding to the $\delta(v - v_e)$ component in the Landau theory.[32] With increasing distance the multiple scattering distribution dominates while the zero-scattering and single-scattering plasmon peaks disappear. In all cases the agreement between the Landau theory and the MC simulation is satisfactory. Figures 6(a)–6(c) display the angular distributions for the same distances of propagation. The bin size in the MC simulation is $\Delta\theta = 0.56°$. At small distances the influence of small-angle scattering due to inelastic scattering is visible. Here the angular distribution produced by the Goudsmit-Saunderson theory with only elastic scattering taken into account deviates markedly from the distribution including both elastic and inelastic deflections for angles $\lesssim 5°$. This is directly related to the average transverse momentum transfer for inelastic collisions $\langle P_\perp^i \rangle = 0.7$ a.u. [$\tan^{-1}(\Delta P_\perp^i / v_e) \simeq 3.2°$]. $\langle \Delta P_\perp^i \rangle$ is considerably larger than the longitudinal momentum transfer responsible for the stopping power $\langle \Delta P_\parallel^i \rangle \simeq -0.27$ a.u. The recoiling (quasi)particles (electrons or plasmons) are therefore emitted at large angles. Since, on the other hand, the average momentum transfer for elastic collision $\langle \Delta P_\perp^e \rangle \simeq 2.7$ a.u. is large compared to $\langle \Delta P_\perp^i \rangle$, the influence of elastic scattering rapidly dominates at larger angles and larger distances of propagation thereby justifying the separability approximation [Eq. (22)] for many applications. The overall excellent agreement between the stochastic dynamics calculation and the solution to the one-dimensional transport equations lends confidence to the application of the present approach to the nonseparable transport problem in the presence of a Coulomb field.

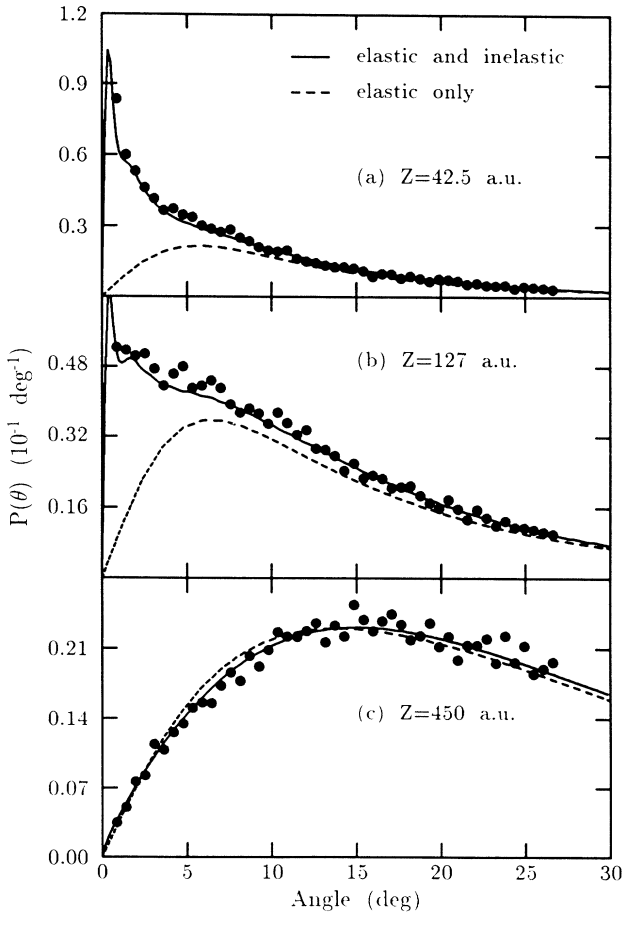

FIG. 6. Angular straggling distributions of free electrons for path length (a) $Z = 42.5$, (b) $Z = 127$, and (c) $Z = 450$ a.u.; ——, Goudsmit-Saunderson theory; — — —, Goudsmit-Saunderson theory for elastic scattering only; ●, Langevin equation (bin size $\Delta\theta = 0.56°$).

V. COULOMB TRANSPORT

A. Velocity space distributions

The drastic effect of the presence of the Coulomb field is illustrated in the two-dimensional velocity distributions at path length $Z = 42.5$ and 127 a.u. with and without a strong Coulomb field ($q = 18$, $L = 3$) (Fig. 7). Each diagram represents ensembles of initially 2000 test particles each of which is marked by a dot. The most remarkable difference is a rapid and almost "isotropic" diffusion of the initial distribution located at $v_P = 12.5$ a.u. This key observation leads to two consequences: First, the motion in the presence of a Coulomb field displays an increased *instability* to which we refer in the following as Coulomb defocusing. The instability is related to the intrinsically

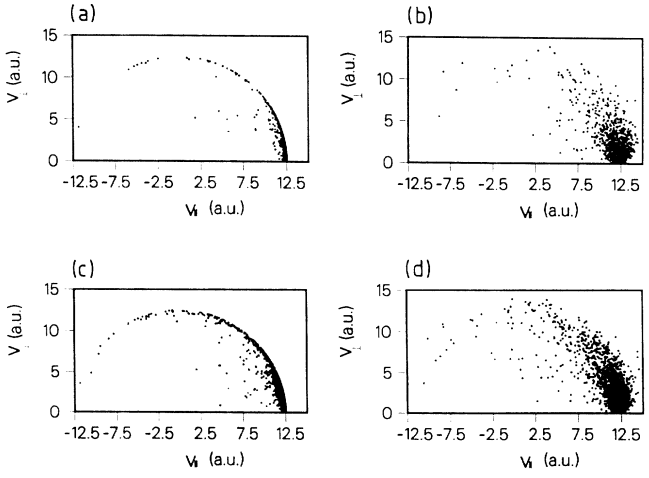

FIG. 7. Two-dimensional velocity space distributions after a path length of (a) and (b) $Z = 42.5$ and (c) and (d) $Z = 127$. (a) and (c) are for free electrons, (b) and (d) for convoy electrons with $L = 3$, $q = 18$. Note that all particles of the zero-scattering peak are represented by one dot.

chaotic dynamics of impulsively perturbed atomic systems.[37] Second, the near isotropic expansion indicates that collisions can lead to both energy loss and energy gain. The classification of electron-core and electron-electron collisions as "elastic" and "inelastic" becomes obsolete even though we will continue to use this terminology for reasons of convention. The underlying mechanism is the coupling of the collisional momentum and of the local orbital momentum. The change in energy per collision as measured in the laboratory frame is given by

$$\Delta E = \tfrac{1}{2}(\mathbf{v}_P+\mathbf{v}+\Delta\mathbf{P})^2-\tfrac{1}{2}(\mathbf{v}_P+\mathbf{v})^2$$

$$=\mathbf{v}_P\cdot\Delta\mathbf{P}+\frac{\Delta P^2}{2}+\mathbf{v}\cdot\Delta\mathbf{P} \tag{41a}$$

or, equivalently, in the projectile frame by

$$\Delta E' = \mathbf{v}\cdot\Delta\mathbf{P}+\Delta P^2/2\ . \tag{41b}$$

The first two terms in (41a) are unchanged compared to free-electron scattering, while the third depends on the local momentum $\mathbf{v}(\mathbf{r})$ of the electron on the Coulomb orbit. The local momentum is of the order of the Compton width q/L [or $q/L\sqrt{\alpha}$, see Eq. (9) and Fig. 1]. In contrast to the sum of the first two terms, which assures slowing down ($\Delta E<0$), the third term is not negative definite. For large q/L the latter can change the overall sign of ΔE resulting in an energy gain. The strong influence of the Coulomb force is most pronounced at short distances of propagation. Due to the growing distance from the center of the Coulomb force the phase-space evolution becomes increasingly free-particle-like. Coulomb defocusing effects are therefore transient. Another important observation related to (41b) is that for $\Delta E'<0$ transitions to negative-energy states in the projectile, i.e., bound orbits in the moving projectile, become possible.

A detailed comparison between Coulomb evolution and free-particle evolution is shown in Figs. 8–11 for energy and angular straggling distributions. The energy straggling spectra are completely altered even in weak fields $q/L\simeq 0.33$ (Fig. 8). The zero-loss peak is reduced since collision events which are energy conserving for free particles are energy changing in the presence of the Coulomb field. The peaks due to σ and π plasmon excitations are completely smeared out. The reason is that the Compton width is larger than the characteristic longitudinal momentum transfer associated with plasmon excitation [see Eq. (37)]. In order to restore part of the plasmon structure and to illustrate the smooth transition from the free-particle to the Coulomb transport we have chosen in Fig. 9 an unphysically small Compton width parameter ($q/L=0.016$ e.g., $q=0.05$, $L=3$). The σ plasmon peak is now largely unchanged while the spectrum is distorted only in the near vicinity of the zero-loss peak. Our present results readily explain why all experimental studies of convoy electrons to date, unlike free-electron emission, do not display any discrete loss structures despite the available high-energy resolution.[7,38]

The energy distributions (Figs. 7–9) display a high-energy component of electrons faster than the initial convoy velocity $v_e=v_P$. This is an additional manifestation of the Compton width. It is instructive to trace the origin of the high-energy component $v_e>v_P$. From (41a) it is obvious that for $q/L<v_P$ an energy gain in the laboratory frame requires $\Delta\mathbf{P}$ to be approximately parallel to the orbital velocity $\mathbf{v}(r)$ and perpendicular to $\mathbf{v}_P$. Therefore the transverse components $\Delta\mathbf{P}_\perp$ of both the elastic and inelastic collisions cause energy-gaining collisions. This fact underlines the importance of the transverse component $\Delta P_\perp^i$ of the inelastic momentum transfer. Since $\langle\Delta P_\perp^i\rangle<\langle\Delta P_\perp^e\rangle$, we expect that the immediate vicinity of the cusp peak $v_e\gtrsim v_P$ energy gain is primarily due to inelastic collisions, while large energy gains are associated with the elastic channel. This expectation is confirmed by a computer simulation (Fig. 10) where we have selectively switched off either one of the two collision mechanisms. The inelastic channel displays a pronounced asymmetry of the low- and high-energy wings, which is the obvious consequence of the presence of the negative-definite terms in Eq. (41a).

The phase-space distribution is profoundly affected by another feature not directly visible in the energy and an-

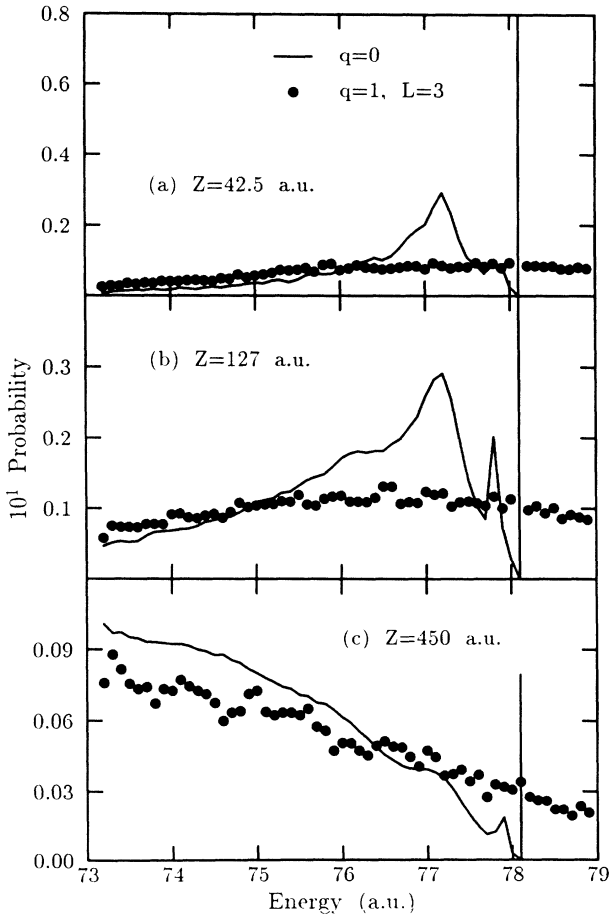

FIG. 8. Comparison of the energy distribution $P(E)\Delta E$, ($\Delta E=0.1$ a.u.) for free electrons (——) and convoy electrons [●, ($q=1$, $L=3$)] after a path length of (a) $Z=42.5$, (b) $Z=127$, and (c) $Z=450$ a.u.

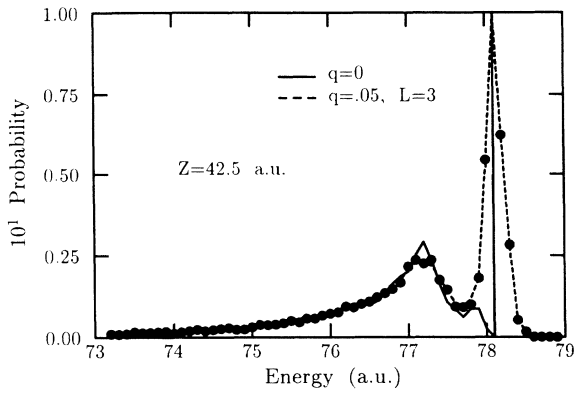

FIG. 9. Comparison of the energy distribution $P(E)\Delta E$, ($\Delta E=0.1$ a.u.) for free electrons (——) and convoy electrons [●, ($q=0.05$, $L=3$)] after a path length of $Z=42.5$ a.u. The singular zero-scattering peak is not to scale.

gle distributions of (continuum) electrons: According to (41b) transitions to negative-energy states in the projectile, i.e., the capture of the continuum electron into a bound orbit becomes possible for $\Delta E'<0$. This decay channel for convoy electrons is important for highly charged ions with a high density of states below threshold. An analytic estimate for the recapture probability of convoy electrons has been developed[39] showing that capture is a universal function of q/L which approaches 0.5 for isotropically distributed $\Delta\mathbf{P}$ in the limit $q/L \gg \langle \Delta P \rangle$. The transient trapping of continuum electrons in negative-energy states determines in the long-term behavior of convoy-electron attenuation.

In marked contrast to the drastic modification of energy straggling the angular straggling distribution is largely unaffected (Fig. 11). A notable exception is the distribution for highly charged ions at small angles and small distances of propagation where the Coulomb distribution develops a "hole." This reduction of angular scattering

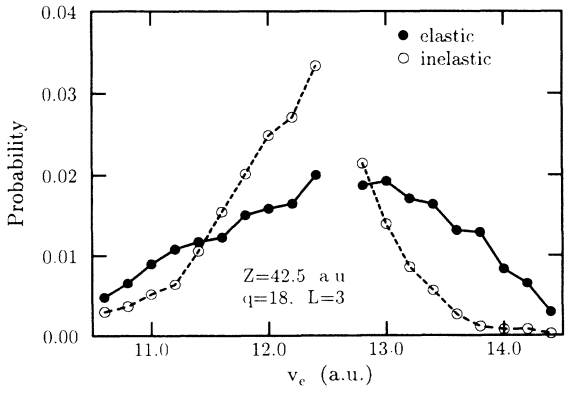

FIG. 10. Wings of the velocity distribution of convoy electrons $P(v_e)\Delta v_e$ after a path length of $Z=42.5$; ●, only "elastic" collisions; ○, only "inelastic" collisions; peak region suppressed for clarity (bin size $\Delta v_e=0.2$ a.u.).

probability is predominantly due to capture of continuum electrons into bound states. Note that the inelastic electron-electron scattering predominantly mediates transitions into negative-energy states in the projectile frame and depletes the angular distribution at small angles. The relative stability of the angular distribution with respect to Coulomb distortions can be understood with help of a simple analytic estimate similar to the one given by Eq. (41). We note first that electron scattering far away from the Coulomb center is free-electron-like. The largest distortion is expected for collisions near the pericenter. For an initial parabolic orbit with its major axis aligned along the beam axis, the convoy scattering angle in the laboratory frame, θ_L^c, can be shown to be

$$\tan\theta_L^c = \frac{v_y(0)+\Delta P}{v_P}\left[1-\frac{1}{[1+(2\Delta E' L^2/q^2)]^{1/2}}\right], \quad (42)$$

where $v_y(0)=p_0$ is the tangential velocity at the pericenter [see Eq. (10)]. In order to maximize the distortion effect and to exclude capture, ΔP is assumed to be parallel to $v_y(0)$. Accordingly,

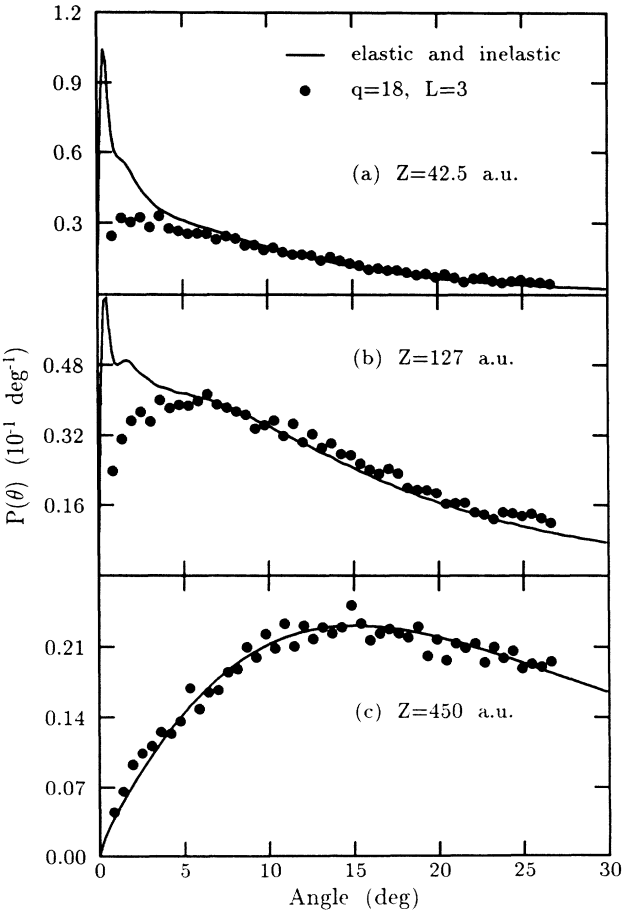

FIG. 11. Comparison of angular straggling distributions of free electrons (——) and of convoy electrons [●, ($q=18$, $L=3$)].

$$\Delta E' = v_y(0)\Delta P + \Delta P^2/2 \tag{43}$$

is the energy given in the projectile frame. Expressed in terms of reduced variables

$$g = \Delta P / v_P \ , \tag{44}$$

$$s = \Delta P / p_0 \ , \tag{45}$$

Eq. (42) becomes

$$\tan\theta_L^c = g\left[1+\frac{1}{s}\right]\left[1-\frac{1}{[1+8(s+s^2/2)]^{1/2}}\right] . \tag{46}$$

The corresponding scattering angle for free electrons is given by

$$\tan\theta_L^f = g \ . \tag{47}$$

The modification due to the presence of the Coulomb field depends only on s, i.e., the ratio of the transverse momentum transfer to the characteristic orbital momentum p_0. The deflection function [Eq. (46)] for different $p_0 = 2q/L$ as a function of ΔP is displayed in Fig. 12. Note that the slope of the deflection function $(d\theta/d(\Delta P))^{-1}$ determines the angular straggling. At large angles the slope is little affected while an enhancement of $d\theta/d(\Delta P)$ for small momentum transfers and consequently a depletion of the small scattering probability is observed. In the limit $s \to \infty$ the maximum enhancement of the convoy scattering angles relative to free electrons can be shown to be

$$\theta_L^c = 4\theta_L^f \ , \tag{48}$$

that is, the amplification of the deflection angle reaches a saturation value which is independent of q. This enhancement is, however, responsible only for a small fraction of probability loss at small angles (Fig. 11), the reason being that the phase-space density associated with the most favorable conditions for enhanced angular defocusing discussed above is very small. In other words, chances to find a comet near the pericenter (perihelion) at the moment the collision occurs are slim.

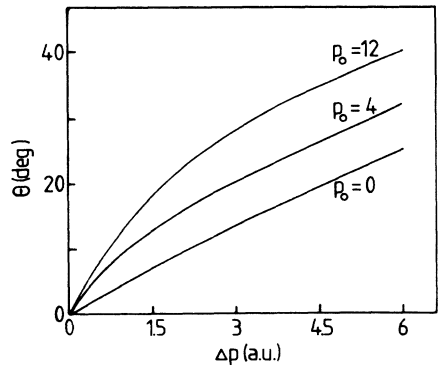

FIG. 12. Deflection functions for free electrons ($p_0 = 0$) and for convoy electrons [$p_0 > 0$, see Eqs. (40) and (41)] as a function of the transverse momentum transfer.

B. Transport coefficients

The presence of the Coulomb forces has a dramatic influence on transport coefficients such as mean free paths, stopping power, and energy straggling. We emphasize that these modifications are transient. Since the unbound convoy electrons ultimately leave the Coulomb interaction region, the transport coefficients converge to the free-particle values as $Z \to \infty$ (or $t \to \infty$). All transport coefficients discussed in the following are measured at $Z = 0$ (or $t = 0$) where Coulomb effects are maximal. Figure 13 displays the $t = 0$ elastic and inelastic mean free paths for convoy electrons. Both display a moderate enhancement, which is obviously a universal function of the Compton width parameter q/L. The net enhancement is the result of two counteracting mechanisms: MFP's for free electrons [see Eq. (29)] in the present energy range are monotonically increasing functions proportional to v_e^β ($1.5 \lesssim \beta \leq 2$). Since the local velocity of the electron in the Coulomb orbit is larger than the corresponding velocity for free electrons, the MFP's are enhanced. This is partially compensated by the corresponding path-length enhancement associated with the motion in a Coulomb orbit. It should be emphasized that the Coulomb-enhanced MFP's are not directly related to

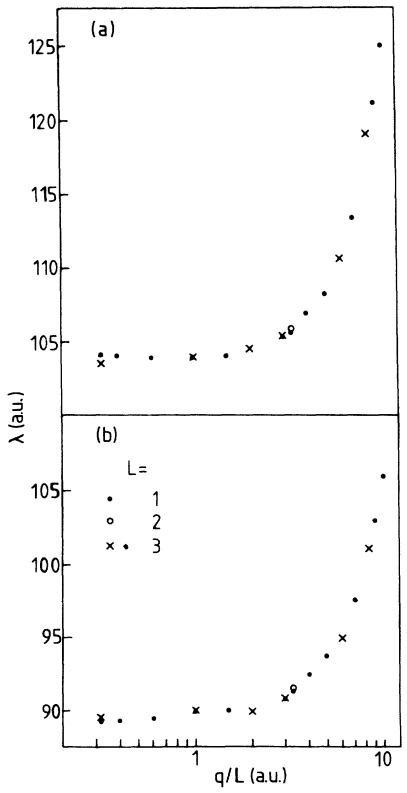

FIG. 13. Modification of the (a) elastic and (b) inelastic mean free paths for convoy electrons and an initial distribution given by Eq. (10) as a function of the reduced variable q/L; ●, $L = 1$; ○, $L = 2$; ×, $L = 3$.

the previously reported enhanced "MFP's" for convoy electrons.[8-11] Precisely speaking, the latter are attenuation lengths which will be considered in Sec. V C. A characteristic time constant within which Coulomb modifications persist can be estimated by the transit time through the region $r \lesssim r_c$ [see Eq. (7)] to be of the order of

$$t_c \simeq \frac{\alpha}{4}\frac{L^3}{q^2} = \frac{\alpha}{4\omega_\infty} . \tag{49}$$

For $\alpha = 10$ and most cases of interest $t_c \ll \langle \Delta t \rangle$, i.e., the strong modifications are confined to a time interval smaller than the interval within which the first collision occurs. The enhancement of the MFP's is therefore of little relevance for the comparison with the experiment.

Dramatic changes can be observed for the stopping power and energy straggling displayed as a function of the reduced variable q/L (Fig. 14). Both stopping power and energy straggling converge to the free-electron limit as $q/L \to 0$. The stopping power [Fig. 14(a)] becomes negative for $q/L \gtrsim 4$. This change of sign is an immediate consequence of the presence of the heavily weighted $v > v_P$ component in the energy straggling distribution for highly charged ions (Fig. 7). While the value of the stopping power itself changes rapidly within t_c [Eq. (49)], the effects of an initially negative stopping power are clearly visible for much larger periods of time and are of importance for the velocity distribution of convoy electrons. For large q/L energy straggling is enhanced by factors $\gtrsim 10$. It is the size of the straggling parameter that is responsible for the complete smearing-out of the plasmon peaks and the approximately symmetric energy (velocity) distribution around the cusp peak in contrast to the pronounced asymmetry predicted by models based on free-electron transport.[40,41] As expected from our analysis of the angular distributions, the angular straggling coefficient agrees with the free-electron value within the statistical uncertainty.

C. Convoy attenuation

The experimentally accessible transport length for convoy electrons is the attenuation length l_c. It is defined by the distance with which the number of convoy electrons within a given collection volume has decreased to e^{-1} of the initial value. The corresponding attenuation of free electrons is denoted by l_f. The attenuation length satisfies the inequality

$$l_{c,f} \geq \lambda , \tag{50}$$

where the total mean free path is given by

$$\lambda^{-1} = \lambda_e^{-1} + \lambda_c^{-1} . \tag{51}$$

Equation (50) follows from the fact that scattering events ejecting the electron out of the collection volume constitute a proper subset of all collisions which determine λ. In the following a near-cubic collection volume with volume $\simeq (2\Delta v)^3$ centered about $\mathbf{v}_P$,

$$\begin{aligned} &v_P - \Delta v \leq v_e \leq v_P + \Delta v , \\ &0 \leq \theta_e \leq \theta_0 \simeq \Delta v / v_P , \end{aligned} \tag{52}$$

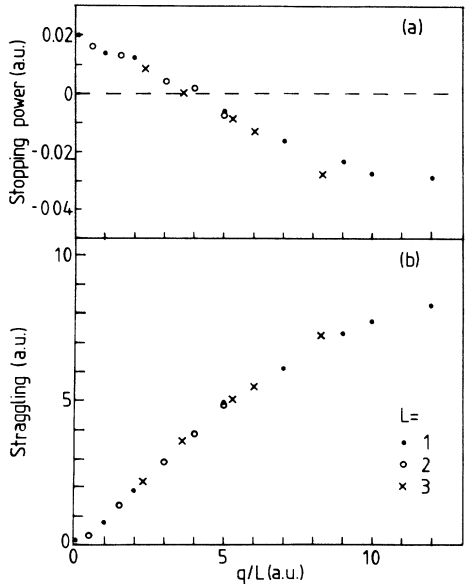

FIG. 14. (a) Stopping power and (b) energy straggling parameter for convoy electrons [initial distribution Eq. (10)] as a function of the reduced variable q/L; ●, $L=1$; ○, $L=2$; ×, $L=3$.

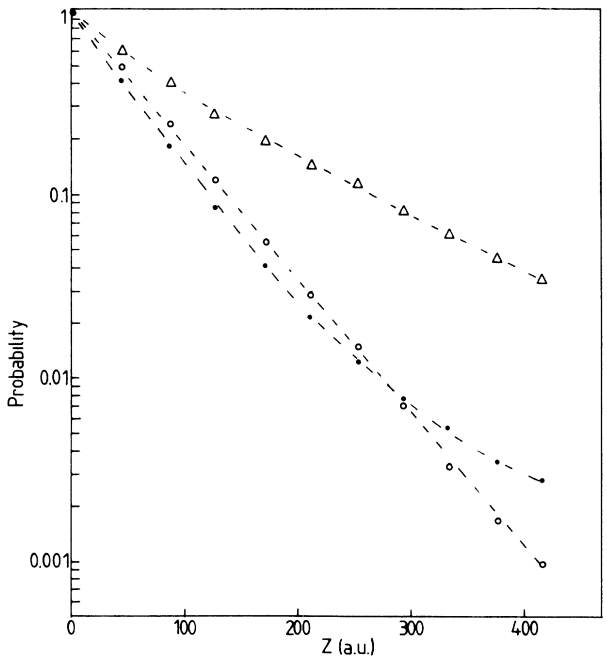

FIG. 15. Attenuation of free electrons (○) and convoy electrons (●), ($q=18$, $L=3$) for a collection volume with $\Delta v = 0.25$. Also shown is the attenuation (Δ) of phase-space correlated electrons (i.e., convoy electrons plus bound electrons).

is chosen. Accordingly, the inequality (50) approaches equality in the limit $\Delta v \to 0$. The concept of the attenuation length tacitly assumes an exponential depletion of the initial intensity. For free electrons an exponential decay law is appropriately observed (Fig. 15). In the presence of a Coulomb field a drastically different picture emerges. The convoy electrons are initially depleted exponentially but at a faster rate than free electrons, which is a direct consequence of Coulomb defocusing. For large path length (or larger evolution times) the decay pattern changes dramatically. A long-time tail develops which is due to both the delayed release of the recaptured electrons in subsequent ionizing collisions and the redistribution and slowing down of high-energy continuum electrons with velocities $v_e \geq v_P$. Both effects are directly related to the presence of the strong Coulomb field and can be identified as a "focusing" effect. The result is the suppression of convoy-electron attenuation at large path lengths. The effect of Coulomb focusing can be made more obvious by studying the attenuation of all phase-space correlated electrons, i.e., the sum of all bound and convoy electrons, also shown in Fig. 15. The corresponding attenuation length l_{cc} is considerably larger than l_f. In the present case we have $l_{cc}/l_f \simeq 2.6$.

The deviation from a monoexponential decay law for convoy electron occurs only at distances where the convoy intensity is reduced by a factor $\simeq 10^2$. In spite of the difficulties discussed, the attenuation length l_c therefore provides a meaningful description for convoy-electrons extinction. The dependence of l_c on the size of the collection volume is displayed in Fig. 16 for different q/L. l_c is found to be close to the mean free path λ for large q/L. In view of Eq. (41) and the results for energy straggling, this can be easily understood in terms of Coulomb defocusing: The enhanced energy transfer per collision due to the coupling to the local momentum in the Coulomb field causes the removal of electron from the collection volume in a larger number of collisions than for free electrons. The present results lead to two important conclusions: The convoy attenuation length is reduced and for small collection volumes approximately equals the total MFP of a free electron contrary to the notion of an enhanced attenuation length. Interpretation of experimental findings[8-11] requires the analysis of the approach to excitation equilibrium instead. Furthermore, the convoy yield as a function of collection volume (Fig. 16) may provide direct and easily accessible evidence for Coulomb defocusing. The increase of attenuation length with increasing Δv is strongly suppressed for large q/L. We therefore propose an experimental study of the yield as a function of collection volume and path length.

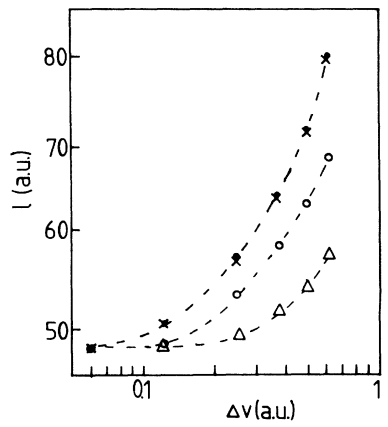

FIG. 16. Attenuation length as a function of the linear dimension, Δv of the collection volume for different $p_0 = 2q/L$; ●, $p_0 = 0$; ×, $p_0 = 0.033$; ○, $p_0 = 0.67$; △, $p_0 = 12$.

VI. CONCLUDING REMARKS

We have analyzed the solution of a phase-space master equation describing electron transport in the presence of a Coulomb field provided by an ion in the near proximity. We have tested the method of test-particle discretization and solved a stochastic differential equation by comparison with the free-electron transport problem for which exact numerical solutions of the master equation are feasible. We found excellent agreement lending confidence in the present approach.

The presence of the Coulomb field induces profound changes of the transport behavior which can be summarized as Coulomb (de)focusing effects. Defocusing effects include a drastic enhancement of energy straggling, the averaging-out of plasmon loss structures, and the reduction of zero-scattering peak and of the attenuation length. Coulomb focusing effects manifest themselves as an initially increased MFP, a negative stopping power, the buildup of a bound-state population, and an enhanced correlation length. Other aspects presently under investigation[39] include dynamical screening field effects, the approach to charge state and excitation equilibrium, and quantum effects on the transport behavior.

We finally note that the present approach has a broader scope than just the application to the ion-solid interaction. With minor modifications the theory can be applied to a variety of problems in different subfields such as the l mixing and destruction of Rydberg atoms in ambient gases[42] and the injections of comets out of the Oorth cloud into the solar system under the influence of gravitational encounters.[43]

ACKNOWLEDGMENTS

We acknowledge illuminating discussions with Jim Ashley, Chris Bottcher, Rufus Ritchie, and Ivan Sellin. This work was supported in part by the National Science Foundation and by the U.S. Department of Energy, Office of Basic Energy Sciences, Division of Chemical Sciences, under Contract No. DE-AC05-840R21400 with Martin Marietta Energy Systems, Inc.

APPENDIX

Using the same notation as in Eq. (10) the Kepler equations for elliptic orbits ($E < 0$) are given by[29]

$$\theta = u - \epsilon \sin u \ , \tag{A1}$$

$$r(u) = a(1 - \epsilon \cos u) \ , \tag{A2}$$

$$x(u) = a(\cos u - \epsilon) \ , \tag{A3}$$

$$y(u) = a(1-\epsilon^2)^{1/2} \sin u \ , \tag{A4}$$

$$\omega_n = \frac{q^2}{n^3} \ , \tag{A5}$$

$$v_x(u) = -\frac{q}{n} \frac{\sin u}{1 - \epsilon \cos u} \ , \tag{A6}$$

$$v_y(u) = \frac{q}{n}(1-\epsilon^2)^{1/2} \frac{\cos u}{1 - \epsilon \cos u} \ . \tag{A7}$$

The eccentricity is given by

$$\epsilon = \left[1 + \frac{2EL^2}{q^2} \right]^{1/2} , \tag{A8}$$

the effective Bohr radius by

$$a = n^2/q \ , \tag{A9}$$

and the energy by

$$E = -\frac{q^2}{2n^2} \ . \tag{A10}$$

Similarily for hyperbolas ($E > 0$) we have

$$\theta = \epsilon \sinh u - u \ , \tag{A11}$$

$$r(u) = a(\epsilon \cosh u - 1) \ , \tag{A12}$$

$$x(u) = a(\epsilon - \cosh u) \ , \tag{A13}$$

$$y(u) = a(\epsilon^2 - 1)^{1/2} \sinh u \ , \tag{A14}$$

$$\omega_n = \frac{q^2}{n^3} \ , \tag{A15}$$

$$v_x(u) = -\frac{q}{n} \frac{\sinh u}{(\epsilon \cosh u - 1)} \ , \tag{A16}$$

$$v_y(u) = \frac{q}{n}(\epsilon^2 - 1)^{1/2} \frac{\cosh u}{\epsilon \cosh u - 1} \ . \tag{A17}$$

Equations (A8) and (A9) remain unchanged while

$$E = \frac{q^2}{2n^2} \ . \tag{A18}$$

[1] H.-D. Betz, D. Röschenthaler, and J. Rothermel, Phys. Rev. Lett. **50**, 34 (1983); H. D. Betz, in *Forward Electron Ejection in Ion Collisions,* Vol. 213 of *Lecture Notes in Physics,* edited by K. O. Groeneveld *et al.* (Springer-Verlag, Berlin, 1984), p. 115; H.-D. Betz, R. Höppler, R. Schramm, and W. Oswald, Nucl. Instrum. Methods B **33**, 185 (1988).

[2] G. Dehmelt, A. Georgiadis, L. V. Gerdtell, D. Sträter, and P. van Brentano, Phys. Lett. **29A**, 193 (1982).

[3] K. Dybdal, J. Sorensen, P. Hvelpund, and H. Knudsen, Nucl. Instrum. Methods Phys. B **13**, 581 (1986).

[4] C. Can, R. J. Maurer, B. Bandong, and R. L. Watson, Phys. Rev. A **35**, 3244 (1987).

[5] Y. Yamazaki *et al.*, Phys. Rev. Lett. **61**, 2913 (1988).

[6] J. Burgdörfer and C. Bottcher, Phys. Rev. Lett. **61**, 2917 (1988).

[7] S. D. Berry, S. B. Elston, I. A. Sellin, M. Breinig, R. DeSerio, C. E. Gonzalez-Lepera, and L. Liljeby, J. Phys. B **19**, L149 (1986); J. P. Gibbons, S. B. Elston, C. E. Gonzalez-Lepera, R. DeSerio, M. Breinig, O. Heil, H. P. Hülskötter, H. Rothard, I. A. Sellin, and C. R. Vane, Nucl. Instrum. Methods B **40/41**, 53 (1989).

[8] I. A. Sellin *et al.*, *Forward Electron in Ion Collisions* (Ref. 1), p. 109.

[9] R. Schramm, P. Koschar, H. D. Betz, M. Burkhard, J. Kemmler, O. Heil, and K. O. Groeneveld, J. Phys. B **18**, L507 (1985).

[10] G. Schiwietz, D. Schneider, and J. Tanis, Phys. Rev. Lett. **59**, 1561 (1987).

[11] J. Kemmler, O. Heil, H. Rothard, K. Kroneberger, S. Lencinas, and K. O. Groeneveld, Acta. Phys. Hungar. **65**, 135 (1989).

[12] J. Neufeld and R. H. Ritchie, Phys. Rev. **98**, 1632 (1955).

[13] P. Echenique, W. Brandt, and R. H. Ritchie, Phys. Rev. B **33**, 43 (1979).

[14] J. Burgdörfer, in *Proceedings of the Third Workshop on High Energy Ion-Atom Collisions,* Vol. 294 of *Lecture Notes in Physics,* edited by D. Berenyi and G. Hock, (Springer-Verlag, Berlin, 1988), p. 344; J. Burgdörfer, in *Proceedings of the Sixteenth International Conference on the Physics of Electronic and Atomic Collisions, New York, 1989,* AIP Conf. Proc. No. 205, edited by A. Dalgarno, R. S. Freund, M. S. Lubell, and T. B. Lucatorto (AIP, New York, 1990).

[15] D. Gemmell, J. Remillieux, J. Poizat, M. Gaillard, R. Holland, and Z. Vager, Phys. Rev. Lett. **34**, 1420 (1975); A. Faibis, R. Kaim, I. Plesser, and Z. Vager, Nucl. Instrum. Methods **170**, 99 (1980).

[16] Y. Yamazaki *et al.*, CERN Report No. CERN-PSCC 87-39 (unpublished), p. 108; CERN Report No. CERN-PSCC 87-40 (unpublished), p. 108; J. Burgdörfer, J. Wang, and J. Müller, Phys. Rev. Lett. **62**, 1599 (1989); and in Oak Ridge National Laboratory Conference Report No. CONF-8909210, 1990, available from National Technical Information Service, p. 239.

[17] E. Williams, Proc. R. Soc. London Ser. A **169**, 531 (1931); **125**, 470 (1929).

[18] S. Goudsmit and J. L. Saunderson, Phys. Rev. **57**, 24 (1940).

[19] L. Landau, J. Phys. (Moscow) **8**, 1 (1944).

[20] U. Fano, Annu. Rev. Nucl. Sci. **13**, 1 (1963).

[21] P. Sigmund and K. Winterbon, Nucl. Instrum. Methods **119**, 541 (1974); S. Tougard and P. Sigmund, Phys. Rev. B **25**, 4452 (1982).

[22] J. Ashley, C. Tung, and R. Ritchie, Surf. Sci. **81**, 409 (1979); C. Martin, E. Arakawa, T. Callcott, and J. Ashley, J. Electron Spectrosc. Relat. Phenom. **35**, 307 (1985); J. Ashley, J. Cowan, R. Ritchie, V. E. Anderson, and J. Hoelz, Thin Films **60**, 361 (1979); J. Ashley, J. Electron Spectrosc. Relat. Phenom. **28**, 177 (1982).

[23] C. Tung, Surf. Interface Anal. **11**, 69 (1986).

[24] C. Kwei, Thin Solid Films **111**, 83 (1984).

[25] H. Bichsel, Rev. Mod. Phys. **60**, 663 (1988), and references therein.

[26] M. Breinig *et al.*, Phys. Rev. A **25**, 3015 (1982); K. O. Groeneveld, W. Meckbach, I. Sellin, and J. Burgdörfer, Comments At. Mol. Phys. **14**, 187 (1984).

[27]R. Abrines and I. C. Percival, Proc. Phys. Soc. London **88**, 861 (1966); **88**, 873 (1966); R. Olson, in *Electronic and Atomic Collisions,* edited by H. Gilbody, W. Newell, F. Read, and A. Smith (North-Holland, Amsterdam, 1988), p. 271; C. Reinhold and R. E. Olson, Phys. Rev. A **39**, 3861 (1989).

[28]R. Shakeshaft and L. Spruch, Phys. Rev. Lett. **41**, 1037 (1978); J. Briggs and M. Day, J. Phys. B **13**, 4797 (1980); J. Burgdörfer, M. Breinig, S. Elston, and I. Sellin, Phys. Rev. **28**, 3277 (1983).

[29]L. Landau and I. Lifshitz, *Lehrbuch der theoretischen Physik* (Akademie-Verlag, Berlin-Ost, 1970), Vol. 1.

[30]For a definition of Euler angles, see M. Rose, *Elementary Theory of Angular Momentum* (Wiley, New York, 1957).

[31]N. van Kampen, *Stochastic Processes in Physics and Chemistry* (North-Holland, Amsterdam, 1981).

[32]S. Lencinas, J. Burgdörfer, J. Kemmler, O. Heil, K. Kroneberger, N. Keller, H. Rothard, and K. O. Groeneveld, Phys. Rev. A **41**, 1435 (1990); J. Kemmler, Ph.D. thesis, Universität Frankfurt, 1988 (unpublished).

[33]H. Bischel (unpublished).

[34]J. Ganachaud and M. Cailler, Surf. Sci. **83**, 498 (1979).

[35]H. Raether, *Excitation of Plasmons and Interband Transitions by Electrons,* Vol. 88 of *Springer Tracts in Modern Physics* (Springer, Berlin, 1980).

[36]J. R. Herring and E. Merzbacher, J. Elisha Mitchell, Sci. Soc. **73**, 267 (1957); K. Ispirian, A. Margarian, and A. Zverev, Nucl. Instrum. Methods **117**, 175 (1974).

[37]J. Burgdörfer, Nucl. Instrum. Methods B **42**, 500 (1989).

[38]A. Gladieux and A. Chateau-Thierry, Phys. Rev. Lett. **47**, 786 (1981).

[39]J. Burgdörfer (unpublished).

[40]J. Kemmler, S. Lencinas, P. Koschar, O. Heil, H. Rothard, K. Kroneberger, G. Szabo, and K. O. Groeneveld, Nucl. Instrum. Methods B **33**, 317 (1988).

[41]R. Barrachina, A. Goni, P. Focke, and W. Meckbach, Nucl. Instrum. Methods B **33**, 330 (1988).

[42]F. Dunning and R. Stebbings, Comments Mol. Phys. **10**, 9 (1980); C. Burkhart, R. Corey, W. Garver, J. Leventhal, M. Allegrini, and L. Moi, Phys. Rev. A **34**, 80 (1986).

[43]R. Sagdeev and G. Zaslavsky, Nuovo Cimento **97**, 119 (1987); B. Marsden, Z. Sekania, and E. Everhart, Astron. J. **83**, 64 (1978).